Vol 15 No 5, May 2006
1009-1963/2006/15(05)/1101-09

Chinese Physics

© 2006 Chin. Phys. Soc.
and IOP Publishing Ltd

Polar interface and surface optical vibration spectra in multi-layer wurtzite quantum wires: transfer matrix method*

Zhang Li(张 立)†

Department of Mechanism and Electronic, Panyu Polytechnic, Panyu 511483, China

(Received 29 October 2005; revised manuscript received 1 March 2006)

The polar interface optical (IO) and surface optical (SO) phonon modes and the corresponding Fröhlich electron–phonon–interaction Hamiltonian in a freestanding multi-layer wurtzite cylindrical quantum wire (QWR) are derived and studied by employing the transfer matrix method in the dielectric continuum approximation and Loudon's uniaxial crystal model. A numerical calculation of a freestanding wurtzite GaN/AlN QWR is performed. The results reveal that for a relatively large azimuthal quantum number m or wave-number k_z in the free z-direction, there exist two branches of IO phonon modes localized at the interface, and only one branch of SO mode localized at the surface in the system. The degenerating behaviours of the IO and SO phonon modes in the wurtzite QWR have also been clearly observed for a small k_z or m. The limiting frequency properties of the IO and SO modes for large k_z and m have been explained reasonably from the mathematical and physical viewpoints. The calculations of electron–phonon coupling functions show that the high-frequency IO phonon branch and SO mode play a more important role in the electron–phonon interaction.

Keywords: interface and surface optical phonons, multi-layer cylindrical heterostructures, wurtzite quantum wires
PACC: 7865K, 7138, 6320K

1. Introduction

The lattice dynamic properties of polar semiconductor heterostructures, such as planar quantum wells (QWs), cylindrical quantum wires (QWRs) and spherical quantum dots (QDs) *et al*, have been extensively studied both experimentally and theoretically.[1−34] This is mainly due to the fact that at room and higher temperatures, the scattering of electrons by optical phonons plays a dominant role in determining various electronic properties; and the electron–phonon interactions and scattering also govern a number of important properties of quantum heterostructures, including hot-electron relaxation rates, interband transition rates, and room-temperature exciton lifetimes, etc. With the great progress of crystal-growing technology, such as hydride vapour phase epitaxy (HVPE), molecular-beam epitaxy (MBE) and metal-organic chemical vapour deposition (MOCVD), not only the planar wurtzite heterostructures, but also the curved wurtzite heterostructures have been synthesized successfully.[16−21] Thus the investigations of the optical phonons have been extended from the cubic QW and QWR systems,[1−11] and planar wurtzite QW systems[22−26] to the quasi-one-dimensional (Q1D) wurtzite QWR systems.[16−21,27]

The Q1D structures of wurtzite nitride QWR with wide band-gaps covering from ultraviolet to red are ideal electronic bound systems for the fundamental study of their physical properties and also for the fabrication of new optoelectronic nanodevices.[16−21] For example, the self-organized ZnO and GaN QWR ultraviolet lasers have revealed a narrow emission linewidth and relatively low threshold.[16−19] The Raman scattering spectra of wurtzite QWRs[28,29] have also shown more complicated phonon vibration properties than those of zinc-blende QWs or QWRs. Both the theoretical and the experimental work reveal that the phonon modes and electron–phonon interactions in the wurtzite heterostructures are obviously differ-

*Project supported by the National Natural Science Foundation of China (Grant Nos 60276004 and 60390073) and the Natural Science Foundation of Guangzhou Education Bureau, China (Grant No 2060).
†E-mail: zhangli-gz@263.net

ent from those in cubic lattice QW systems due to the anisotropy of wurtzite crystal.[22−26] On the other hand, because of the reduction in the dimensionality and the anisotropy of wurtzite structure, the properties of optical phonon modes in Q1D wurtzite QWRs have more distinct phonon branches.[22−27] Up to now, the polar phonon vibration properties of these Q1D wurtzite QWR have not been understood sufficiently. The main aim of the present work is to solve one type of important polar oscillating mode, i.e. the interface optical (IO) and surface optical (SO) phonon modes, in a freestanding wurtzite multi-layer cylindrical QWR system.[27]

In the previous studies of the polar optical-phonons in wurtzite planar heterostructures, the dielectric continuum (DC) model and Loudon's uniaxial crystal model have been widely adopted.[22−26] Moreover, the experimental results of angular dispersion of polar phonons and Raman scattering in wurtzite planar heterostructures have been proven to be in good agreement with the calculations based on the DC model and Loudon's uniaxial crystal model.[30] Therefore, we study the IO phonon modes in a multi-layer wurtzite QWR model within the framework of the DC model and Loudon's uniaxial crystal model in the present paper.

In order to more explicitly and conveniently understand the significance of the present work, it is necessary to briefly discuss the differences and the relationship between Ref.[27] and this work. The differences and relationship can be summarized into the four points as follows. (i) The physical model investigated in Ref.[27] is obviously different from that in the present work. In Ref.[27], a wurtzite GaN nanowire placed in the AlN dielectric matrix has been studied. Thus there was only one GaN/AlN cylindrical hetero-interface in that nanowire system, and the infinite polar dielectric surrounding was assumed for simplicity. In the present paper, a wurtzite coaxial cylindrical QWR model with n-layer polar materials is investigated. It is obvious that there are (n-1) hetero-interfaces (or -surfaces) in the present QWR system. Furthermore, compared with the case of Ref.[27], a very practical nonpolar dielectric matrix, i.e. vacuum environment, is adopted in the present investigation. (ii) The methods to study the IO (and SO) phonon modes in the two papers are also different. The common algebraic method was used for the investigation of IO modes in the nanowire in Ref.[27], while the transfer matrix method is employed to deal with the IO and SO modes in a multi-layer wurtzite cylindrical heterostructure system for convenience in the present research. Thus the present theoretical scheme seems more concise and explicit. (iii) The results obtained in Ref.[27] are apparently distinct from those presented in this work. For example, there exist not only the IO phonon modes, but also the SO phonon modes in the present paper, but only the IO phonon modes are observed in Ref.[27]. Moreover, the degenerating behaviours of IO and SO modes are more prominent in the wurtzite QWRs in vacuum than in wurtzite nanowire.[27] These features and differences in the two papers are mainly due to their using different physical models. (iv) Based on the above analysis, the present theoretical work can be looked on as a generalization of the previous studies regarding the IO phonon modes in Q1D wurtzite QWRs with a certain layer-number. Furthermore, the present theoretical scheme and results can be directly applied to many important but complicated Q1D wurtzite multi-layer QWR systems, such as standard single cylindrical heterostructures,[27] and inhomogeneous coupling QWRs composed of the group III nitrides.

The rest of this paper is organized as follows. The IO (SO) phonon dispersion relations and the Fröhlich electron-IO (-SO) phonon interaction Hamiltonian in a freestanding n-layer cylindrical wurtzite QWR are deduced in Section 2. The numerical results for the dispersion relation and the electron–phonon coupling functions in a chosen GaN/AlN QWR are presented and discussed in Section 3. Finally, the main results and the significance of the theory described in the present work are summarized in Section 4.

2. Theory

Let us consider a freestanding multi-layer cylindrical wurtzite QWR model with a radius $R_{\rm i}$. We take the z-axis along the direction of the c-axis of the wurtzite material. And the radial and axial directions are denoted by t and z, respectively. Considering the case of free vibrations (the charge density $\rho = 0$) in the media and using the Maxwell equations, we have the relationship including the electric displacement vector $\boldsymbol{D}$, which is given by[24−27]

$$\begin{aligned}\nabla \cdot \boldsymbol{D} =& -\nabla^2[\varepsilon(\omega)\Phi(\boldsymbol{r})] \\ =& -\varepsilon_0\left\{\varepsilon_{\rm t}(\omega)\left[\frac{1}{\rho}\frac{\partial}{\partial\rho}\left(\rho\frac{\partial}{\partial\rho}\right)\right.\right. \\ &\left.\left.+\frac{1}{\rho^2}\frac{\partial^2}{\partial\varphi^2}\right]+\varepsilon_z(\omega)\frac{\partial^2}{\partial z^2}\right\}\Phi(\boldsymbol{r}) = 0\,, \quad (1)\end{aligned}$$

where $\varepsilon(\omega)$ is the dielectric function tensor, and $\Phi(\boldsymbol{r})$ is the electrostatic potential of polar optical phonons. In order to solve the equation conveniently, we define a function $\gamma_i(\omega) = \mathrm{sign}[\varepsilon_{zi}(\omega)\varepsilon_{ti}(\omega)]\sqrt{\varepsilon_{zi}(\omega)/\varepsilon_{ti}(\omega)}$ as given in Ref.[27]. Based on the discussion in Refs.[22–24], we know that, when $\gamma_i(\omega) < 0$ the phonon modes correspond to the vibrate waves. On the contrary, when $\gamma_i(\omega) > 0$, they correspond to the decaying waves. In terms of the properties of IO phonon modes, we know that $\gamma_i(\omega)$ should be positive values in all the media of the QWR systems. Thus the frequencies of IO phonon modes in the freestanding wurtzite GaN/AlN multi-layer QWRs must fall into the three ranges:[27] $\omega_{t\mathrm{T}2} \sim \omega_{z\mathrm{T}1}$, $\omega_{t\mathrm{T}1} \sim \omega_{z\mathrm{L}2}$ and $\omega_{t\mathrm{L}2} \sim \omega_{z\mathrm{L}1}$ (the subscripts $i = 1, 2$ refer to the GaN and AlN materials, respectively).

For the IO phonons in a freestanding n-layer wurtzite QWR, the solution of Eq.(1), i.e. the electrostatic potential of IO modes can be written as

$$\Phi(\boldsymbol{r}) = \sum_{i=1}^{n}\sum_{m,k_z} \mathrm{e}^{\mathrm{i}m\varphi}\mathrm{e}^{\mathrm{i}k_z z}\{[A_i I_m(\gamma_i k_z \rho) + B_i K_m(\gamma_i k_z \rho)]\theta(\rho - R_{i-1})\theta(R_i - \rho)\}\,. \quad (2)$$

In Eq.(2), $\theta(x)$ is the step function, and $K_m(x)$ and $I_m(x)$ are the modified Bessel function of the first kind and the modified Bessel function of the second kind, respectively. The continuity of the phonon potential functions and their normal components of electric displacement to interfaces $\rho = R_i$ $(i = 1, 2, 3 \ldots, n-1)$ imply

$$\begin{cases} \Phi_i^{m,k_z}(\boldsymbol{r})|_{\rho=R_i} = \Phi_{i+1}^{m,k_z}(\boldsymbol{r})|_{\rho=R_i}\,, \\ \varepsilon_{ti}\dfrac{\partial\Phi_i^{m,k_z}(\boldsymbol{r})}{\partial\rho}\Big|_{\rho=R_i} = \varepsilon_{t,i+1}\dfrac{\partial\Phi_{i+1}^{m,k_z}(\boldsymbol{r})}{\partial\rho}\Big|_{\rho=R_i} \end{cases}, \qquad i = 1, 2, \ldots, n\,. \quad (3)$$

We define the 2×2 matrices

$$\boldsymbol{M}_i = \begin{pmatrix} I_m(\gamma_i k_z R_i) & K_m(\gamma_i k_z R_i) \\ \varepsilon_{ti} I'_m(\gamma_i k_z R_i)|_{\rho=R_i} & \varepsilon_{ti} K'_m(\gamma_i k_z R_i)|_{\rho=R_i} \end{pmatrix}, \quad (4)$$

$$\boldsymbol{M}'_i = \begin{pmatrix} I_m(\gamma_i k_z R_i) & K_m(\gamma_i k_z R_i) \\ \varepsilon_{t,i+1} I'_m(\gamma_i k_z R_i)|_{\rho=R_i} & \varepsilon_{t,i+1} K'_m(\gamma_i k_z R_i)|_{\rho=R_i} \end{pmatrix} \quad (5)$$

and the vectors

$$\boldsymbol{C}_i = \begin{pmatrix} A_i \\ B_i \end{pmatrix}, \quad (6)$$

then Eqs.(3) can be expressed by

$$\boldsymbol{M}_i\boldsymbol{C}_i = \boldsymbol{M}'_i\boldsymbol{C}_{i+1}\,, \quad (i = 1, 2, ..., n-1)\,. \quad (7)$$

By solving the inverse matrix, it is easy to derive the relation

$$\boldsymbol{C}_i = \left(\prod_{j=i}^{n-1}\boldsymbol{D}_j\right)\boldsymbol{C}_n\,, \quad (8)$$

where

$$\boldsymbol{D}_i = \boldsymbol{M}_i^{-1}\cdot\boldsymbol{M'}_i\,. \quad (9)$$

In particular, when $i = 1$, by using Eq.(8), one can obtain

$$\boldsymbol{C}_1 = \left(\prod_{j=1}^{n-1}\boldsymbol{D}_j\right)\boldsymbol{C}_n\,. \quad (10)$$

Moreover, we notice that $A_n = B_1 = 0$ in Eq.(2). By using this condition and Eq.(10), the following relation is obtained:

$$B_1 = \left[\prod_{j=1}^{n-1}\boldsymbol{D}_j\right]_{2,2} = 0\,, \quad (11)$$

which just gives the dispersion relation of the IO (or SO) phonon modes in the multi-layer cylindrical heterostructures. The coupling coefficients in the electrostatic potential function (2) can be expressed by B_n, and they are given by

$$A_i = \left[\prod_{j=i}^{n-1}\boldsymbol{D}_j\right]_{1,2} B_n = g_i B_n\,, \quad (12)$$

$$B_i = \left[\prod_{j=i}^{n-1}\boldsymbol{D}_j\right]_{2,2} B_n = h_i B_n\,. \quad (13)$$

Using Eqs.(12) and (13), the phonon potential function (2) can be further rewritten as

$$\Phi(\boldsymbol{r}) = \sum_{i=1}^{n}\sum_{m,k_z} B_n \mathrm{e}^{\mathrm{i}m\varphi}\mathrm{e}^{\mathrm{i}k_z z}\{[g_i I_m(\gamma_i k_z \rho) + h_i K_m(\gamma_i k_z \rho)]\theta(\rho - R_{i-1})\theta(R_i - \rho)\}\,. \tag{14}$$

The polarization fields for the IO and SO phonon modes of the system are given by

$$\begin{aligned}\boldsymbol{P}^{\mathrm{IO,SO}}_{m,k_z} =& \frac{1-\varepsilon}{4\pi}\nabla\,\Phi(\boldsymbol{r})_{m,k_z} = \frac{B_n}{4\pi}\sum_{i=1}^{n}[(1-\varepsilon_{ti})\nabla_\rho + (1-\varepsilon_{ti})\partial_z] \\ &\times\{\mathrm{e}^{\mathrm{i}m\varphi}\mathrm{e}^{\mathrm{i}k_z z}[g_i I_m(\gamma_i k_z\rho) + h_i K_m(\gamma_i k_z\rho)]\theta(\rho - R_{i-1})\theta(R_i-\rho)\}\,.\end{aligned} \tag{15}$$

It is easy to have the orthogonal relationship for the polarization vector of IO (SO) phonons $\boldsymbol{P}^{\mathrm{IO,SO}}_{m,k_z}$, i.e.

$$\int \boldsymbol{P}^{*\mathrm{IO,SO}}_{m',k'_z}\cdot\boldsymbol{P}^{\mathrm{IO,SO}}_{m,k_z}\mathrm{d}^3\boldsymbol{r} = \frac{|B_n|^2}{16\pi^2}\sum_{i=1}^{n}[(1-\varepsilon_{zi})^2\mathrm{Inz}(i,m,k_z) + \gamma_i^2(1-\varepsilon_{ti})^2\mathrm{Int}(i,m,k_z)]\delta_{m,m'}\delta_{k'_z,k'_z}\,, \tag{16}$$

where

$$\mathrm{Inz}(i,m,k_z) = 2\int_{R_{i-1}}^{R_i}\rho\mathrm{d}\rho[g_i^2 I_m^2(\gamma_i k_z\rho) + h_i^2 K_m^2(\gamma_i k_z\rho) + 2g_i h_i I_m(\gamma_i k_z\rho)K_m(\gamma_i k_z\rho)]\,, \tag{17}$$

$$\begin{aligned}\mathrm{Int}(i,m,k_z) =& \int_{R_{i-1}}^{R_i}\rho\mathrm{d}\rho\{g_i^2[I_{m-1}^2(\gamma_i k_z\rho) + I_{m+1}^2(\gamma_i k_z\rho)] + h_i^2[K_{m-1}^2(\gamma_i k_z\rho) + K_{m+1}^2(\gamma_i k_z\rho)] \\ &+ 2g_i h_i[I_{m+1}(\gamma_i k_z\rho)K_{m+1}(\gamma_i k_z\rho) - I_{m-1}(\gamma_i k_z\rho)K_{m-1}(\gamma_i k_z\rho)]\}\,.\end{aligned} \tag{18}$$

By using the orthogonal relation and following the steps similar to those in Refs.[8–10], it is easy to obtain the free IO and SO phonon field as

$$H_{\mathrm{IO,SO}} = \sum_{m,k_z}\hbar\omega\left[b_m^\dagger(k_z)b_m(k_z) + \frac{1}{2}\right], \tag{19}$$

where $b_m^\dagger(k_z)$ and $b_m(k_z)$ are creation and annihilation boson operators for IO and SO phonons of the (m,k_z)th mode. The Fröhlich Hamiltonian describing the interaction between an electron and the IO (SO) phonons is given by

$$H_{e-\mathrm{IO,SO}} = -\sum_{m,k_z} \Gamma^{\mathrm{IO,SO}}_{m,k_z}(\rho)[\mathrm{e}^{\mathrm{i}m\varphi}\mathrm{e}^{\mathrm{i}k_z z}b_m(k_z) + H.c.]\,, \tag{20}$$

where $\Gamma^{\mathrm{IO,SO}}_{m,k_z}(\rho)$ is the coupling function, which describes the coupling strength of a single electron at the position ρ with the (m,k_z)-th IO (SO) mode, and is defined as

$$\Gamma^{\mathrm{IO,SO}}_{m,k_z}(\rho) = N_m \times \sum_{i=1}^{n}\mathrm{e}^{\mathrm{i}m\varphi}e^{\mathrm{i}k_z z}[g_i I_m(\gamma_i k_z\rho) + h_i K_m(\gamma_i k_z\rho)]\theta(\rho - R_{i-1})\theta(R_i - \rho) \tag{21}$$

with

$$|N_{k_1,k_2}| = \sqrt{\frac{2\hbar\omega e^2}{k_z^2 L}}\left\{\sum_{i=1}^{n}[\bar{\varepsilon}_{zi}\mathrm{Inz}(i,m,k_z) + \gamma_i^2\bar{\varepsilon}_{ti}\mathrm{Int}(i,m,k_z)]\right\}^{-1}. \tag{22}$$

In Eq.(22), $\bar{\varepsilon}_{ui}$ is an effective dielectric function of the ith-layer material, which is defined as

$$\bar{\varepsilon}_{ui} = \left(\frac{1}{\varepsilon_{ti} - \varepsilon_{ti0}} - \frac{1}{\varepsilon_{ti} - \varepsilon_{ti\infty}}\right)^{-1}, \qquad u = t,z; i = 1,2,...,n\,. \tag{23}$$

3. Numerical results and discussion

In this section, we discuss the dispersion frequencies of IO and SO phonons and their electron–phonon coupling functions for a chosen GaN/AlN QWR placed in vacuum with the radii being 5 nm, 5 nm and ∞. The material parameters used in our calculation are cited from Ref.[22].

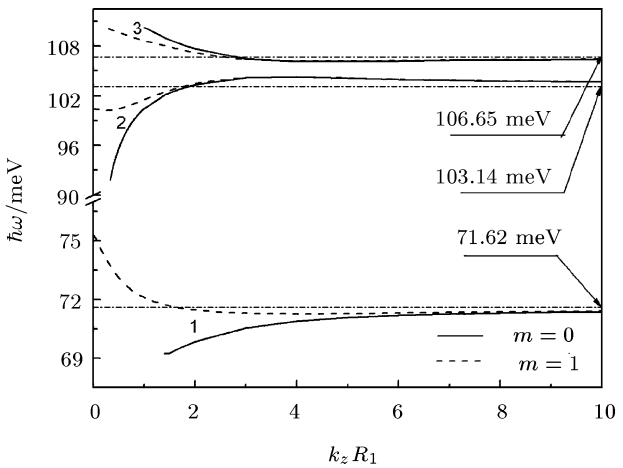


Fig.1. Dispersion frequencies $\hbar\omega$ of the IO and SO phonon modes as a function of k_z when $m = 0$ (solid lines) and $m = 1$ (dash lines), respectively.

Figure 1 plots the dispersion frequencies $\hbar\omega$ of the IO and SO phonon modes as a function of the phonon wave-number k_z in the z-direction in the wurtzite QWR system when the azimuthal number m is kept at 0 (solid lines) and 1 (dash lines), respectively. We can see from the figure that for a given azimuthal quantum m and relatively large k_z ($k_z R_1 > 1.4$), there are three branches of IO and SO phonon modes labelled respectively by 1, 2 and 3 according to the order of increasing frequency in the system, which means that Eq.(11) usually has three solutions for ω. When k_z is small, the dispersions are more prominent. It is also noticed that the frequencies of the low-frequency mode 1 vary between $\omega_{t\mathrm{T1}}$ and $\omega_{z\mathrm{T2}}$, and those of the high-frequency modes 2 and 3 fall into a frequency range from $\omega_{t\mathrm{L1}}$ to $\omega_{z\mathrm{L2}}$, which is similar to the case in wurtzite QW systems,[22–26] but different from the cases in the zinc-blende crystal QW systems [5–8] and QWR systems.[9,10] (In zinc-blende heterostructure systems,[5–10] the frequency values of IO phonon modes fall into two ranges: $\omega_{\mathrm{TO}1} - \omega_{\mathrm{LO}1}$ and $\omega_{\mathrm{TO}2} - \omega_{\mathrm{LO}2}$.) When k_z approaches infinity, the frequencies of these modes converge to three definite constant values 71.62 meV, 103.14 meV and 106.65 meV, respectively (shown by dash-dot lines in Fig.1). Through detailed calculation, we find that the values of the first two frequencies are just the limiting frequencies of IO phonons in wurtzite GaN/AlN planar heterostructure,[22] and the last value is just the frequency of SO phonons in wurtzite AlN/Vacuum heterostructure. This interesting feature is not surprising, but it has a profound physical and mathematical source. From a mathematical point of view, it is well known that the limiting frequencies of IO phonons for large wave numbers in zinc-blende planar heterostructure are determined by Eq.(24) as follows:

$$\varepsilon_1(\omega)/\varepsilon_2(\omega) = -1\,, \tag{24}$$

and those in wurtzite single planar heterostructure can be obtained by solving the following equation[22]

$$\sqrt{\varepsilon_{t1}(\omega)\varepsilon_{z1}(\omega)/\varepsilon_{t2}(\omega)\varepsilon_{z2}(\omega)} = -1\,. \tag{25}$$

On the other hand, we know that, when $x \to \infty$, the functions $I_m(x)$ and $K_m(x)$ approach $\mathrm{e}^x/\sqrt{2\pi x}$ and $\mathrm{e}^{-x}\sqrt{\pi}/\sqrt{2x}$, respectively. By using these relationships, the dispersion Eq.(11) can naturally reduce to the following form:

$$\left(\frac{\varepsilon_{t1}\gamma_1 + \varepsilon_{t2}\gamma_2}{\varepsilon_{t1}\gamma_1 - \varepsilon_{t2}\gamma_2}\right)\left(\frac{\varepsilon_d + \varepsilon_{t2}\gamma_2}{\varepsilon_d - \varepsilon_{t2}\gamma_2}\right) = \exp[-2\gamma_2(R_2 - R_1)k_z]\,. \tag{26}$$

When $k_z \to \infty$, $\exp[-2\gamma_2(R_2 - R_1)k_z]$ approaches zero, which requires the following relationship to hold true, i.e.

$$\varepsilon_{t1}(\omega)\gamma_1/\varepsilon_{t2}(\omega)\gamma_2 = -1 \tag{27}$$

or

$$\varepsilon_{t2}(\omega)\gamma_2/\varepsilon_d = -1\,. \tag{28}$$

Substitute $\gamma_i(\omega)$ into Eq.(27), then the resulting Eq.(27) will have the same form as the Eq.(25). This clearly illustrates the mathematical reason why the limiting frequencies of the IO phonons are the same for very large wave-numbers in wurtzite planar heterostructure and in cylindrical heterostructure systems. Equation (28) just gives a limiting frequency value 106.65 meV. Thus the modes 1 and 2 can be looked on as the IO modes at the interface $\rho = R_1$, and the mode 3 can be treated as the SO mode at the surface $\rho = R_2$, which can be seen more clearly in Fig.3. Furthermore, it is observed obviously that Eqs.(24) and (25) will have the same form if the anisotropy of the wurtzite material is ignored. From the purely physical viewpoint, when the wave number k_z approaches infinity, the wave-lengths of the IO (SO) phonons become very short. On this condition, the IO (SO) phonons cannot distinguish between the planar heterostructure and the curved cylindrical heterostructure.[11] This will directly results in the identical limiting frequencies of IO (SO) phonons for large wave-numbers in wurtzite planar heterostructures and in cylindrical heterostructure systems. From the features of the solid lines for m= 0 and the dash

lines for m= 1, one can find that the frequency dispersion becomes weaker and weaker with the increase of m. A feature obviously different from that in zinc-blende crystal QW and QWR[5−15] is as follows: some modes, such as the modes 1, 2 and 3 for $m = 0$ in the wurtzite QWR can exist only when $k_z R_1$ is over 1.4, 0.33 and 1.0 , respectively. But in the zinc-blende crystal QWs and QWRs,[5−15] these modes always exist, even for a very small k_z.[5−15] This feature completely results from the anisotropy of wurtzite crystals. Detailed calculations show that the modes 1, 2 and 3 for $m = 0$ occur at the frequencies 69.65 meV, 91.83 meV and 110.28 meV, which are very close to the three characteristic frequencies $\omega_{t,\mathrm{T2}}$, $\omega_{t,\mathrm{L1}}$ and $\omega_{z,\mathrm{L1}}$, respectively. By using the definition of $\gamma_i(\omega)$, it can be clearly seen that, when $\omega < \omega_{t,\mathrm{T2}}$ or $\omega > \omega_{t,\mathrm{L1}}$ ($\omega_{z,\mathrm{L1}}$), $\gamma_i(\omega)$ will become negative values and the IO (SO) phonon modes will disappear. The IO (SO) phonon modes will degenerate into the other phonon vibration modes, such as exactly bound modes, quasi-bound modes or propagating modes,[22−26] which have not been fully understood up to now and will be the subject of projected subsequent research.

In order to clearly see the dependence of dispersion frequency $\hbar\omega$ on the quantum number m, the IO (SO) phonon frequencies as a function of m are plotted when k_z is kept equal to $1/R_1$ (Fig.2a) and $2/R_1$ (Fig.2b), respectively. The frequency is a discrete function of quantum number m. Similar to the case in Fig.1, when m is small, the dispersion is more prominent, and with the increase of m, each frequency of the IO (SO) phonon mode also approaches a constant. We also observe that the dispersion of each branch of IO (SO) phonon modes in Fig.2(a) is stronger than that of the corresponding branch of IO (SO) phonon modes in Fig.2(b), which consists with the observation in Fig.1. Furthermore, the degenerate behaviour of mode 1 with $m = 0$ has also been observed in Fig.2(a) and explained above. From a detailed comparison of Fig.2(a) with Fig.2(b), we find that the limiting frequencies of the modes 1, 2, and 3 approach 73.88 meV, 104.57 meV and 108.43 meV, respectively. The limiting frequency values 73.88 and 104.57 meV are just the two solutions of the equation,

$$\varepsilon_{t1}(\omega)/\varepsilon_{t2}(\omega) = -1\,, \tag{29}$$

while the value 108.43 meV is just the root of equation,

$$\varepsilon_{t2}(\omega)/\varepsilon_{d} = -1\,. \tag{30}$$

In fact, for a certain x_0, when$m \to \infty$, the limiting value of the function

$$K_m(x_0)I'_m(x)|_{x=x_0}/K_m(x_0)I'_m(x)|_{x=x_0}$$

approaches 1. By using this relation, the dispersion Eq.(11) can reduce to the same form as that in Eqs.(29) and (30). This feature is obviously different from that in zinc-blende QWR.[9,10] In zinc-blende QWR, the limiting frequencies of IO phonon modes for large azimuthal quantum numbers are the same as the corresponding limiting frequencies for a large k_z. The reason for the difference is obviously due to the anisotropy in wurtzite crystal material and the isotropy in cubic crystal material in the dielectric function. It is found that Eqs.(29) and (24) have similar forms, which illustrates that for a very large azimuthal quantum number m, the dispersion behaviours of IO (SO) phonon modes in wurtzite QWR are similar to those in cubic-crystal single planar heterostructure.[6]

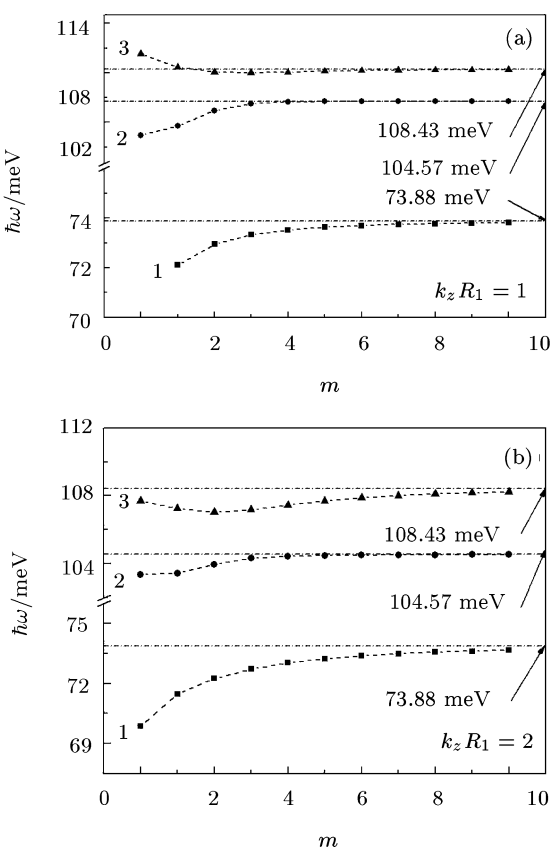


Fig.2. IO and SO phonon frequencies as function of m when $k_z = 1/R_1$ (Fig.2a) and $k_z = 2/R_1$ (Fig.2b).

The electron-IO (SO) phonon coupling functions $I^{\mathrm{IO,SO}}_{m,k_z}(\rho)$ as a function of ρ are depicted in Fig.3 when $k_z = 2/R_1$ and $m = 2$. From the figure it is seen that all the three branches of phonon modes are mainly localized at the interface and the surface, namely, the

modes 1 and 2 are mainly localized at the first interface $R_1 = 5$ nm, and the mode 3 at the surface $R_2 = 10$ nm. So the modes 1 and 2 can be looked on as the IO modes at the first interface, while the mode 3 can be treated as the SO modes at the surface. The maximum absolute value of $\Gamma^{\mathrm{IO,SO}}_{m,k_z}(\rho)$ of the mode 2 or 3 is far larger than that of mode 1, which reveals that the high frequency branches and the SO mode play an important role in the electron-IO (SO) phonon interactions.

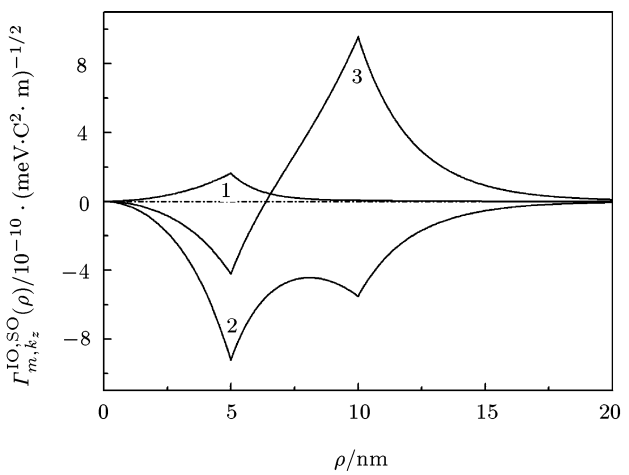


Fig.3. Electron-IO (-SO) phonon coupling function $\Gamma^{\mathrm{IO,SO}}_{m,k_z}(\rho)$ as a function of ρ when $k_zR_1 = m = 2$.

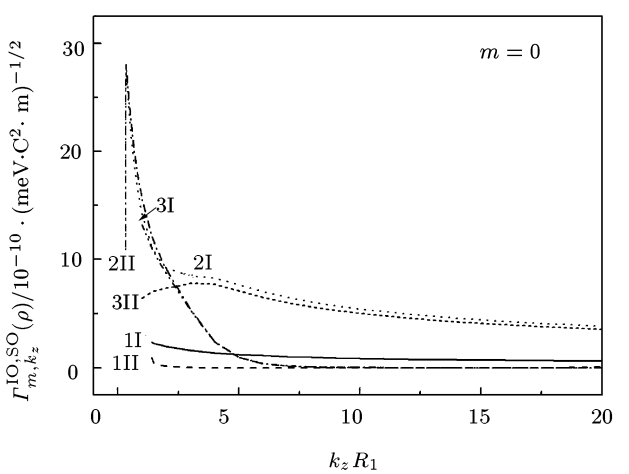


Fig.4. Absolute values $|\Gamma^{\mathrm{IO,SO}}_{m,k_z}(\rho)|$ as a function of k_z for $m = 0$. The symbols "iI" or "iII" represents the ith mode on the first or the second surface, respectively.

In Fig.4, we show the absolute values $|\Gamma^{\mathrm{IO,SO}}_{m,k_z}(\rho)|$ as a function of k_z for $m = 0$. In terms of the analysis in Fig.3, $\rho = 5$ nm and 10 nm are chosen for all of the modes. In fact, the symbols 'I' and 'II' in Fig.4 denote the 1st interface and the 2nd surface, respectively. For example, the symbol '2II' represents the mode 2 on the second surface. From the figure it can be seen that all the curves but for the curves 2II and 3II that each have a maximum respectively at $k_zR_1 = 0.34$ and 3 decrease monotonically. When $k_zR_1 > 5$, the absolute values $|\Gamma^{\mathrm{IO,SO}}_{m,k_z}(\rho)|$ of the curves 1II, 2II and 3I nearly approach 0, while those of the curves 1I, 2I and 3II have certain amplitudes, which just explains why the modes 1 and 2 can be treated as the IO phonon modes at the first interface, and the mode 3 as the SO phonon modes at the surface. On the other hand, it is also observed that the two branches of the phonon modes 2 and 3 with higher frequencies, compared with the lower frequency modes 1, have a strong electron–phonon coupling.

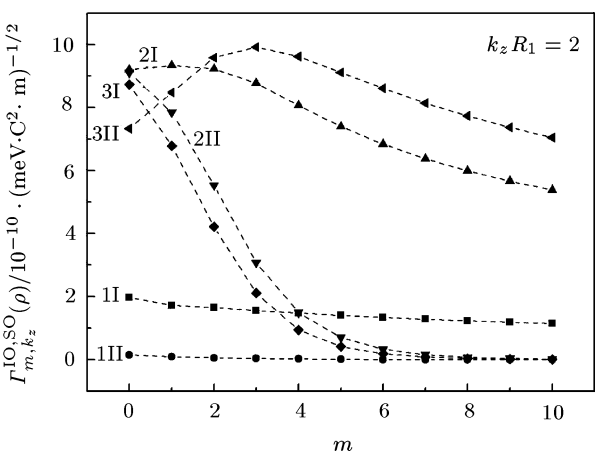


Fig.5. Dependence of the absolute $|\Gamma^{\mathrm{IO,SO}}_{m,k_z}(\rho)|$ on azimuthal quantum number m when k_z is kept equal to $2/R_1$. The symbols 'iI' and 'iII' have the same meanings as those in Fig.4.

Figure 5 plots the dependence of the absolute value $|\Gamma^{\mathrm{IO,SO}}_{m,k_z}(\rho)|$ on the azimuthal quantum number m when k_z is kept equal to $2/R_1$. The symbols 'iI' and 'iII' in the figure denote the same meanings as those in Fig.4. It is observed from the figure that all the curves but for the curve 3II are monotonically regressive with the increase of m. This feature is similar to that in the case of zinc-blende material QWR.[9,10] In the whole range of m, the curve 1I is over curve 1II, and the curve 2I is over curve 2II, so the modes 1 and 2 act as the IO phonon mode at the first interface. This completely consists with the observation in Fig.3 and Fig.4. But for the mode 3, the curve 3II is over the curve 3I when $m \geq 3$. Thus the mode 3 should be looked on as the SO mode, especially for relatively large m and k_z. On the interface, there exist two branches of IO phonon modes, while only one branch of SO phonon mode is localized at the

surface. This feature is obviously different from that in the case of GaN/AlN nanowire,[27] which is due to the difference in dielectric environment between in the two wurtzite cylindrical heterostructure systems. It is also observed that the high frequency modes 2 and 3 play a more important role in the electron–phonon interaction than the low frequency mode. Moreover, when $m > 6$, the electron–phonon coupling function becomes weaker and weaker. Therefore, in the case of weak coupling, it is convenient to adopt a perturbation method to investigate the polaronic effect[31−34] in the wurtzite QWR, which will be our next significant research project.

4. Summary

In this paper, the IO (SO) phonon modes, the orthogonality relation for polarization eigenvector, the dispersion relation, and the Fröhlich electron-IO (SO) phonon interaction Hamiltonian in a multi-layer wurtzite cylindrical QWR system have been deduced and studied by employing the transfer matrix method in the DC approximation and Loudon's uniaxial crystal model. A numerical calculation of a freestanding GaN/AlN wurtzite QWR has been performed, and the calculation mainly is focused on the dispersive relation of IO (SO) phonon modes and the coupling functions between an electron and IO (SO) phonons. The results reveal that, in general, there exist two branches of IO phonon modes localized at the interface and one branch of SO modes localized at the surface in the wurtzite QWR. When k_z or m is small enough, the IO (SO) phonon modes will not appear in the wurtzite QWRs. They will degenerate into the other phonon vibration modes, such as propagating modes and quasi-bound modes[22−27], which are quite different from the cases in zinc-blende QW and QWR systems.[5−15] When k_z or m approaches infinity, the frequencies of the three branches of IO and SO phonon modes converge to the definite constant frequencies determined by corresponding single planar wurtzite heterostructures. The mathematical and physical sources for these properties have been analysed in a deep way. The discussion of the electron–phonon coupling function reveals that the high frequency IO branch and SO modes make more significant contributions to the electron–phonon-interactions. Our investigations also indicate that the anisotropic effects in the wurtzite QWRs result in different dispersion behaviours of IO (SO) phonon modes and electron-coupling properties compared with the cases of zinc-blende QWRs.[9,10] Thus, the anisotropic effects of the wurtzite crystal materials must be taken into consideration, in the study of the relevant physical properties in the wurtzite QWRs, such as electron phonon scattering, polaron effect or bound polaron effect.[31−34]

Acknowledgement

The author would like to thank Professor J J Shi for detailed and valuable discussion.

References

[1] Licari J and Evrard R 1965 *Phys. Rev.* B **15** 2254
[2] Sood K, Menendez J, Cardona M and Ploog K 1985 *Phys. Rev. Lett.* **54** 2111; **54**, 2115
[3] Klein M V 1986 *IEEE J. Quantum Electron.* **QE-22** 1760
[4] Liang X X and Yan Z W 1998 *Surf. Sci.* **400** 232
[5] Wendler L 1985 *Phys. Status Solidi* B **129** 513
[6] Mori N and Ando T 1989 *Phys. Rev.* B **40** 6175
[7] Yu S and Kim K W 1997 *J. Appl. Phys.* **82** 3363
[8] Shi J J, Sanders B C, Pan S H and Goldys E M 1999 *Phys. Rev.* B **60** 16031
[9] Zhang L and Xie H J 2003 *J. Phys.: Condens. Matter* **15** 5881
[10] Xie H J, Chen C Y and Ma B K 2000 *J. Phys.: Condens. Matter* **12** 8623
[11] Enderlein R 1993 *Phys. Rev.* B **47** 2162
[12] Zhang L, Xie H J and Chen C Y 2003 *Chin. J. Phys.* **41** 148
[13] Klein M C, Hache F, Ricard D and Flytzanix C 1990 *Phys. Rev.* B **42** 11123
[14] Roca E, Trallero-Giner C and Cardona M 1994 *Phys. Rev.* B **49** 13704
[15] Cruz R M de la, Teitsworth and Stroscio M A 1995 *Phys. Rev.* B **52** 1489
[16] Choi H J, Johnson J C, He R, Lee S K, Kim F, Pauzauskie P, Goldberger J, Saykally R J and Yang P 2003 *J. Phys. Chem.* B **107** 8271
[17] Goldberger J, He R, Zhang Y, Lee S, Yan H, Choi H-J and Yang P 2003 *Nature* **422** 599
[18] Huang M H, Mao S, Fieck H, Yan H, Wu Y, Kind H, Weber E, Richard R and Yang P 2001 *Science* **292** 5523
[19] Huang W and Jain F 2000 *J. Appl. Phys.* **87** 7354
[20] Shalish I, Temkin H and Narayanamurti V 2004 *Phys. Rev.* B **69** 245401
[21] Yang L, Zhang X, Huang R, Zhang G and Xue C 2005 *Physica* E **25** 582
[22] Shi J J 2003 *Phys. Rev.* B **68** 165335
[23] Shi J J, Chu X L and Goldys E M 2004 *Phys. Rev.* B **70** 115318

[24] Lee B C, Kim K W, Stroscio M A and Dutta M 1998 *Phys. Rev.* B **58** 4860

[25] Gleize J, Renucci M A, Frandon J and Demangeot Fb 1999 *Phys. Rev.* B **60** 15985

[26] Komirenko S M, Kim K W, Stroscio M A and Dutta M 1999 *Phys. Rev.* B **59** 5013

[27] Zhang L, Shi J J and Tansley T L 2005 *Phys. Rev.* B **71** 245324

[28] Liu H L, Chen C C, Chia C T, Yeh C C, Chen C H, Yu M Y, Keller S and DenBaars S P 2001 *Chem. Phys. Lett.* **345** 245

[29] Zhang J, Peng X S, Wang X F, Wang Y W and Zhang L D 2001 *Chem. Phys. Lett.* **345** 372;
Zhang J and Zhang L D 2002 *J. Phys. D: Appl. Phys.* **35** 1481

[30] Gleize J, Demangeot F, Frandon J, Renucci M A, Kuball M, Daudin B and Grandjean N 2001 *Phys. Status Solidi* A **183** 157;
Gleize J, Frandon J, Demangeot, Renucci M A, Kuball M, Hayes J M, Widmann F and Daudin B 2001 *Mater. Sci. Eng.* B **82** 27

[31] Chen C Y, Li W S, Teng X Y and Liang S D 1998 *Physica* B **245** 92

[32] Eerdunchaolu, Li S S and Xiao J L 2005 *Acta Phys. Sin.* **54** 4285 (in Chinese)

[33] Liu Z X, Huang Y C, Liu Y and Jia T Q 1999 *Acta Phys. Sin.* (Overseas Edition) **8** 361

[34] Wang Z B, Wu F L, Chen Q H and Jiao Z K 2001 *Chin. Phys.* **10** 437